Demagnetization Research on PMs in the Halbach Magnetized Pulsed Alternator

Songlin Wu, Shaopeng Wu, *Senior Member*, *IEEE,* Weiduo Zhao, and Shumei Cui

***Abstract*—Demagnetization behavior of Halbach magnetized compensated pulsed alternator (CPA) is studied by using finite element method (FEM) under the different demagnetization factors in this paper. The effect of armature reaction magnetic field and thermal rise on demagnetization of PMs is analyzed. This paper investigates the effect of different demagnetization factors on magnetic field distribution, load current, and no-load phase voltage. A series of dynamic demagnetization points in Halbach array permanent magnet (PM) are evaluated to search the worst working point. Partial demagnetization risk can be represented by the worst working point, and the global demagnetization of the PM is represented by the no-load phase voltage characteristics after discharge. The research results demonstrated that the compensation shield with a certain thickness can increase the discharge current and weaken the demagnetization influence of armature reaction. The demagnetization effect of armature reaction on PMs at high temperatures will be strengthened.**

***Index Terms*—Armature reaction, dynamic demagnetization, finite element method (FEM), pulsed alternator, thermal rise.**

I. INTRODUCTION

PULSED alternator is a kind of pulsed power supply, which is widely applied into electromagnetic launch and laser weapon field [1]-[2]. As we know, the pulsed power supply generally includes inductors, capacitors [3], pulsed alternators and homopolar generators [4]. The pulsed alternators integrate inertial energy storage, pulse shaping and power conditioning into one unit, and it has drawn a great deal of attentions in recent decades due to its high energy density, high repetition rate and high power density [5]-[9].

The electric excitation structure is widely applied into traditional pulsed alternator, but the development of pulsed alternator is limited by the complex electric excitation device [10]. Permanent magnet (PM) pulsed alternator has simpler and more compact structure, and can be manufactured easily [11]-[13]. Compared with the traditional electric excitation pulsed alternator, the brush and slip ring are removed in the Halbach magnetized pulsed alternator, and the friction loss is reduced and the service life of CPA is improved. The PM pulsed alternator performance is limited by the PM material, so the development of PM pulsed alternator is relatively slow.

For the electromagnetic design of CPA, the discharge capacity is the most important consideration. In generally, the discharge ability of CPA includes delivered energy density, energy transfer efficiency. The demagnetization analysis of PMs is an important aspect of the electromagnetic design, and the anti-demagnetization method should be given in order to ensure the CPA operation.

Demagnetization factors include structural stress, thermal rise, external magnetic field (reverse armature reaction magnetic field) and external transient force [14]. Ref. [14] presents a physics-based real-time PM demagnetization model which is a function of physical geometry and material of the PMSM, physics of demagnetization, and the ambient temperature. The model is enabled to dynamically estimate the resultant normal magnetic flux density on the face of PM. Ref. [15] presents a linearized demagnetization model taking into account temperature dependence of the hard magnetic material, but the analysis does not involve the demagnetization of PMs under a large transient current. Ref. [16] investigates the transient magnetic behavior of an interior permanent magnet (IPM) synchronous machine following a large transient current caused by a fault condition, but the thermal rise demagnetization is neglected. Ref. [17] investigates the irreversible demagnetization of a PM brushless dc motor under an inter-turn fault condition and develops a finite-element method-based demagnetization algorithm. Despite the extensive research on demagnetization of PM motors, there are still few studies on demagnetization of large current and high temperature rise for CPAs.

In this paper, demagnetization behavior of thermal rise and armature reaction magnetic field for PMs in the Halbach magnetized compensated pulsed alternator (CPA) is studied by using finite element software, and sectional view of Halbach magnetized CPA as shown in Fig. 1. The linear demagnetization model is used to analyze the partial and global demagnetization for PM during discharge. The research work can be used as the guidance for the design of PM pulsed alternator. Section II introduces the linear demagnetization model of the external magnetic field and thermal rise. Section III studies the effect of armature reaction on the

Manuscript was submitted for review on April 25, 2019.

This work was supported by the Natural Science Foundation of China under Grant 51307031 and part by the Natural Science Foundation of Heilongjiang Province under Grant E2018034 and China Postdoctoral Science Foundation funded project under Grant 2019M651185.

S. Wu, S. Wu and S. Cui are with the Department of Electrical Engineering, Harbin Institute of Technology, Harbin 150080, China (e-mail: wushaopeng@hit.edu.cn; wusonglin297918@126.com; cuism@hit.edu.cn)..

W. Zhao is with the International Academy of the Marine Economy and Technology, University of Nottingham, Ningbo 315000, China (e-mail: Weiduo.Zhao@nottingham.edu.cn).

Digital Object Identifier 10.30941/CESTEMS.2019.00023

demagnetization for the PMs. Section IV studies the demagnetization of the PMs caused by temperature rise. Section V concludes the research results and discussions.

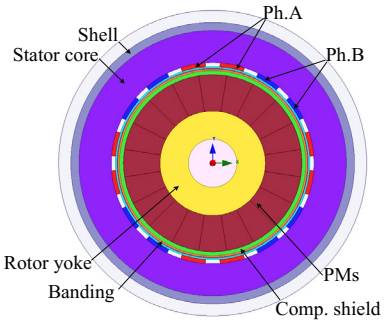

Fig. 1. Sectional view of Halbach magnetized CPA.

II. Linear Demagnetization Model

The CPA as a special alternator which takes advantage of the induced eddy current of compensation structure to compress the armature reaction flux to increase the peak value of output pulse current. PM is used as excitation source of the Halbach magnetized pulsed alternator, so the CPA performance is determined by the development of the PM materials. There are many factors that cause demagnetization of PM, such as chemistry, vibration, external magnetic field, temperature rise, and so on. According to the working mode of CPA, the demagnetization analysis of Halbach array PMs takes into account temperature rise and armature reaction magnetic field in this paper. The Halbach magnetized pulsed alternator is a 4-pole, 2-phase, passively CPA, and the parameters of PM-CPA as shown in Table I.

TABLE I
PARAMETERS OF PM-CPA

Symbols	Parameters	Value
E_r	Kinetic energy of rotor	2 MJ
n_0	Rated speed	12000 rpm
V_0	No-load phase voltage	0.9 kV
I_m	Peak value of load current	$\geqslant$ 60 kA
J_r	Rotating inertia	0.93kg·m^2

The linear demagnetization models of thermal rise and external magnetic field are introduced in this section, and the schematic diagram of linear demagnetization model for PMs are shown in Fig. 2.

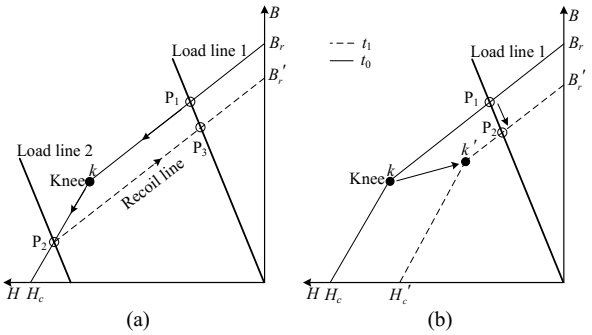

Fig. 2. Linear demagnetization model. (a) External magnetic field. (b) Thermal rise model.

A. External Magnetic Field Demagnetization

External magnetic field demagnetization refers to the process of weakening the magnetic performance due to the change of magnetic moment direction of magnetic domain with external magnetic field. There are many factors for the increase of transient external magnetic field, such as short circuit faults and switch trigger faults. Working point change of PM with different load is shown in Fig. 2(a), and P_1 is the normal working point of the PM (load line 1). The working point of PM changes from P_1 to P_2 when the load changes due to a fault. However, since P_2 is lower than the knee point, the working point changes to P_3 when the fault disappears, not P_1. At the same time, the remanence decreases from B_r to B_r', and the reduced remanence is irreversible demagnetization. Similarly, if P_2 is above the knee point, it can still return to the working point P_1 after the fault is solved. The demagnetization in this process is reversible demagnetization.

B. Thermal Rise Demagnetization

Thermal rise demagnetization refers to the process of decreasing the performance of PMs due to the enhancement of the motion of magnetic domains when the working temperature of PMs rises. PMs will lose their magnetic properties when the temperature rises to a certain value, which is called Curie temperature. The schematic diagram of temperature rise demagnetization as shown in Fig. 2(b), and P_1 is the normal working point of PM. The knee point changes from k to k' when the ambient temperature changes from t_0 to t_1, and the magnetic properties of PM have decreased ($B_r \rightarrow B_r'$, $H_c \rightarrow H_c'$). The working point changes from P_1 to P_2, but the magnetic properties cannot be restored to the initial state (H_c, B_r) when the temperature returns to t_0 and the irreversible demagnetization of the PM has occur. The knee point of the demagnetization curve will appears when the temperature reaches to a certain value, and the knee point value increases with the temperature rise and the lowest working point will be higher and higher, which means that PM is easier to demagnetize.

III. External Magnetic Field Demagnetization

The demagnetization characteristics of PMs under armature reaction during discharge are studied and the partial demagnetization risk of PMs is evaluated in this section. The NMX-S52 material from Hitachi Metals, Ltd. is used to evaluate the demagnetization characteristics of Halbach magnetized CPA based on the linear demagnetization model. Magnetic property curves for NMX-S52 at different temperatures as shown in Fig. 3.

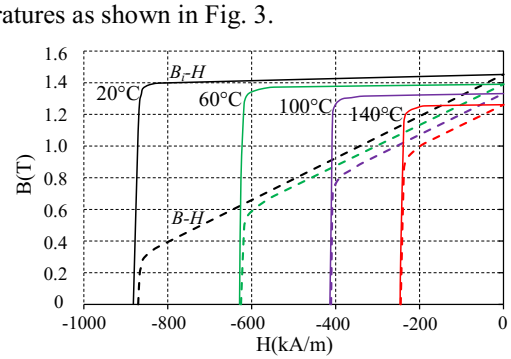

Fig. 3. Magnetic property curves for NMX-S52 at different temperatures.

A. No-Load Finite Element Analysis

In order to increase magnetic flux density of effective air gap, the Halbach array structure is applied into PM CPA. Because Halbach array augments the magnetic field on one side of the array while cancelling the field to near zero on the other side, the rotor yoke can be made of high strength non-ferromagnetic materials, such as glass fiber and carbon fiber. Glass fiber has the advantages of light weight, low cost and high strength, so it is a good choice for the rotor yoke in order to reduce the mass of CPA and to meet strength requirements.

Waveforms of no-load phase voltage and air gap flux density are shown in Fig. 5, the amplitude of no-load phase voltage is about 888.0V, the peak value of air gap flux density is about 1.1T, and the average value of self-inductance for armature windings calculated by using FEA is around 15.3μH.

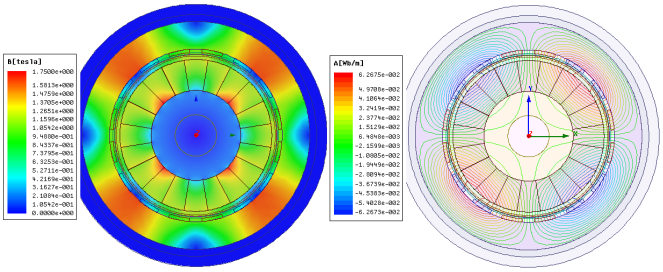

(a) (b)

Fig. 4. No-load magnetic field distribution. (a) Flux density. (b) Flux lines.

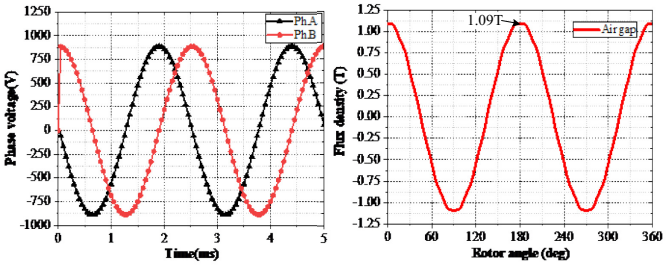

(a) (b)

Fig. 5. Curves of no-load phase voltage and flux density. (a) Phase voltage. (b) Effective air gap flux density.

Dynamic demagnetization points and magnetization direction of Halbach array PMs are shown in Fig. 6(a). Because the distribution of PMs is symmetrical, the demagnetization analysis of PMs in one pole pitch can represent the demagnetization risk of all PMs. The external discharge circuit of two-phase armature winding is shown in Fig. 6(b). The current of armature winding flows through the full-bridge rectifier to the equivalent load, and the pulsed load is simplified to resistance 0.5mΩ and inductance 0.6μH.

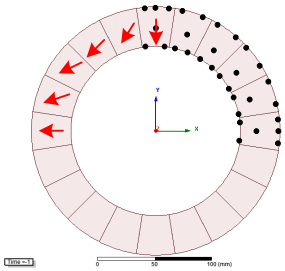

(a) Demagnetization test points distribution.

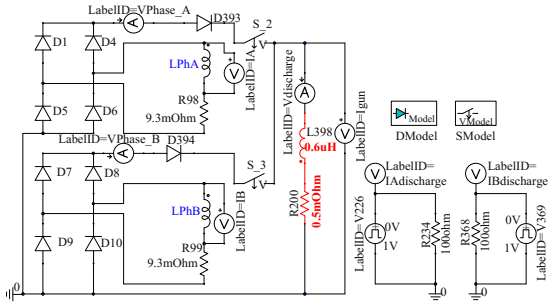

(b) Discharge schematic diagram

Fig. 6. Dynamic demagnetization test points distribution and external circuit of two-phase armature winding in the FEA.

B. Effect of Pulse Duration on Discharge Current

The effect of trigger time on the discharge current is analyzed in this part. In this paper, the pulse duration is controlled by setting different turn-on time and the same turn-off time, which means that the smaller pulse duration, the later the trigger time. Variation of peak value of load current with trigger angle as shown in Fig. 7.

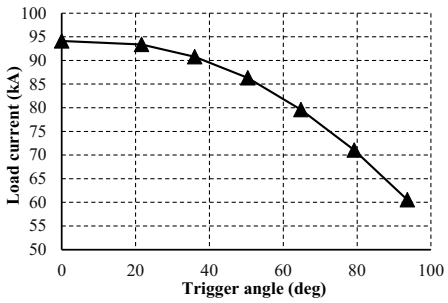

Fig. 7. Variation of peak value of load current with trigger angle.

The peak value of load current decreases with the increase of trigger angle, and the change rate increases when the trigger angle exceeds a certain value. Because of the existence of compensating shield, the demagnetization of PMs under the maximum pulse current is not serious. Therefore, it is not necessary to study the effect of pulse duration with maximum pulse current on demagnetization of the PM.

C. With/Without Compensation Shield

The thickness of compensation shield depends on skin effect, and skin depth calculated by using (1) is about 4.2mm. In order to evaluate the effect of compensation shield on the demagnetization for PMs, the magnetic field, discharge current, and dynamic demagnetization of CPA are analyzed by using finite element software under with or without compensating shield conditions. Based on the discharge circuit as shown in Fig. 6, the simulation results of CPA with or without compensation shield are shown in Fig. 8 (the compensation shield thickness is 5mm). Fig. 8(c) shows comparison of no-load phase voltage waveform in the case where the armature winding is not discharged and discharged under and without compensated shield.

Comparative analysis of load current and dynamic operating points of PM with or without compensation shield from Fig. 8, the peak value of load current is lower when CPA has no compensation shield, but the demagnetization risk of PMs is

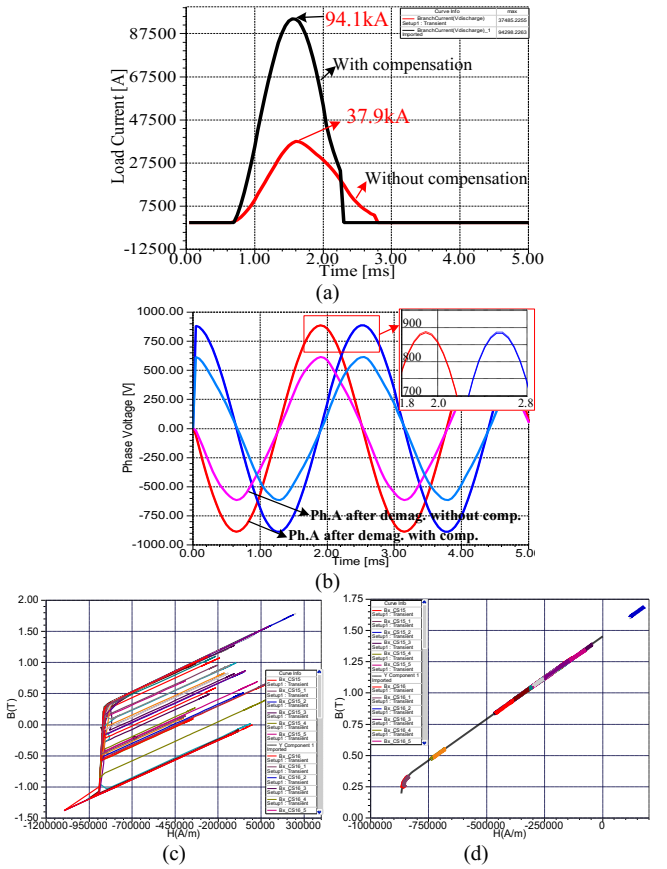

Fig. 8. Comparison of compensated and uncompensated structure. (a) Load current. (b) Phase voltage. (c) Dynamic demagnetization curves without compensation. (d) Dynamic demagnetization curves with compensation.

more serious. The magnetic density distribution of the PMs after discharge of the CPA is shown in Fig. 9. Comparative analysis of magnetic field distribution shows that the compensation shield can weaken the demagnetization risk of PMs and the demagnetization risk on the inner side of PMs with radial magnetization direction is more serious.

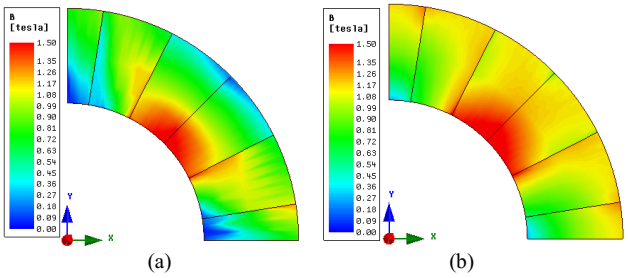

Fig. 9. Flux density distribution of PMs after discharge. (a) Without compensation shield. (b) With compensation shield.

D. Different Compensation Shield Thicknesses

The thickness of compensation shield is determined by skin effect, and the actual thickness of compensation shield usually takes 1.0-2.0 times the skin depth. The skin depth of conductive materials is calculated by using (1).

$$d = \sqrt{\frac{2}{\omega \mu_c \gamma}} \tag{1}$$

where ω is the angular frequency of sinusoidal electromagnetic field, and μ_c, γ are the permeability and conductivity of conductive materials for compensation shield.

The magnetic flux density change of all PMs with different compensation shield thickness are studied in order to accurately know the demagnetization of all PMs during discharge. The global demagnetization of PMs can be represented by the no-load phase voltage change of armature winding after discharge. Variations of no-load phase voltage after discharge and load current with different compensation shield thicknesses as shown in Fig. 10.

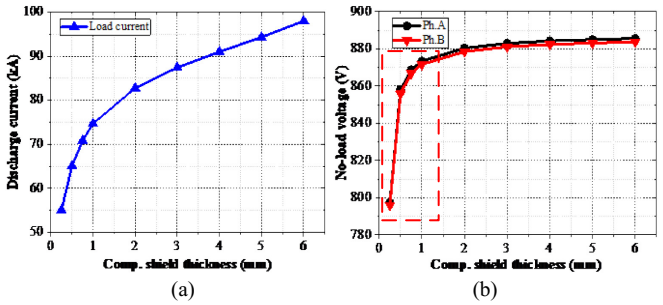

Fig. 10. Variation curves of load current and phase voltage. (a) Load current. (b) No-load phase voltage after discharge.

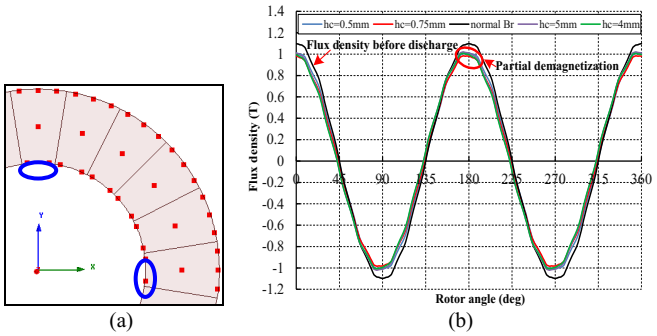

Fig. 11. Local demagnetization points and waveform curves of radial flux density for effective air gap. (a) Maximum partial demagnetization points in the blue circle. (b) Effective air gap flux density.

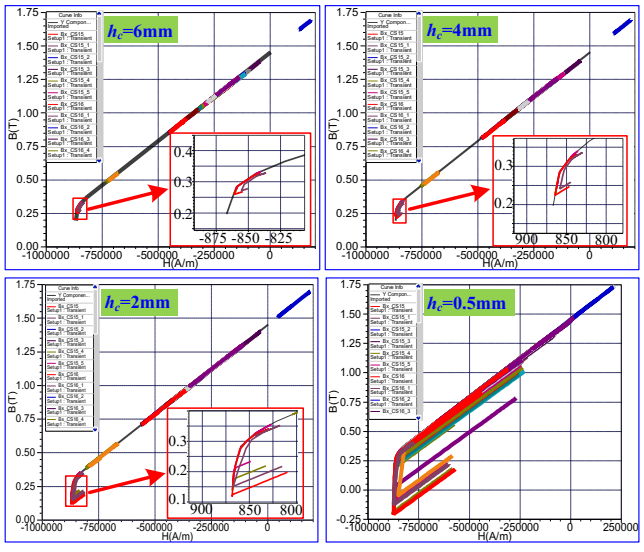

Fig. 12. Dynamic demagnetization curves of test points for PMs with different compensation shield thicknesses.

The variation curve of discharge current with compensation shield thicknesses indicates that the discharge current increases with the increase of compensation shield thickness and the increase decreases. Variation curves of no-load phase voltage

after discharge show that the no-load voltage varies dramatically when the compensation shield thickness ranges 0 to 1mm, but the no-load voltage does not change significantly when the thickness is more than 1mm.

The air gap radial flux density from Fig. 11 shows that the distortion of flux density in the peak value range becomes more serious as the thickness of compensating shield decreases and the demagnetization of PM blocks with radial magnetization direction is more serious (h_c is the compensation shield thickness in the figures). The dynamic demagnetization curves of test points from Fig. 12 shows that although increasing the thickness of compensating shield can reduce the demagnetization risk of PMs, local demagnetization will still occur when the thickness is large enough. The flux density distribution of PMs after discharge when the thickness is 0.5mm or 6mm is consistent with the dynamic demagnetization curves.

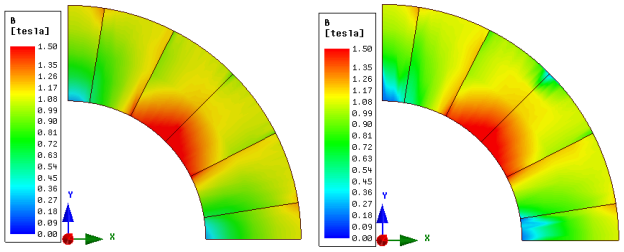

(a) (b)

Fig. 13. Flux density distribution of PMs after discharge with different thicknesses of compensation shield. (a) h_c=6mm. (b) h_c=0.5mm.

E. Multiphase Winding Discharge Demagnetization

The discharge process of two-phase armature winding is greatly complicated. The characteristics of discharge current for the following winding is affected by induced eddy current of compensation shield, though the armature winding axis electrical angle difference is 90°. So the demagnetization analysis of PMs is more difficult when two-phase armature windings are triggered simultaneously. The two-phase discharge case is analyzed in this section, and the simulation results of two-phase winding discharge as shown in Fig. 14.

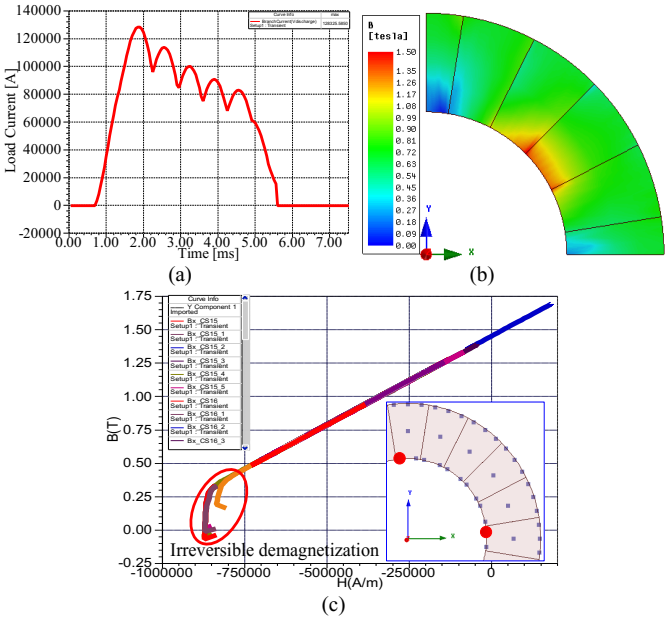

(a) (b)

(c)

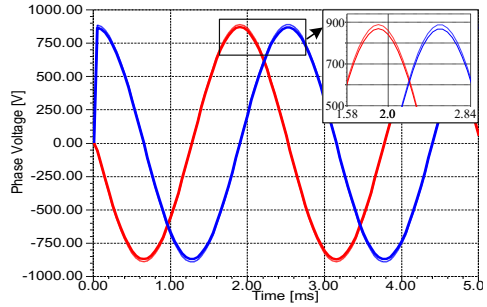

(d)

Fig. 14. Simulation results of two-phase armature winding discharges. (a) Load current. (b) Flux density distribution at the time of CPA discharges. (c) Dynamic demagnetization curves. (d) No-load phase voltage before and after discharge.

The load current waveform of two phase windings are conducted simultaneously as shown in Fig. 14(a), and the peak value of each pulse current decreases gradually and the peak value tends to be stable after a certain time. The inertial energy of the rotor is reduced and the load current tends to be stable during the discharge process. The dynamic demagnetization curves and magnetic flux density waveforms of test points are shown in Fig. 14(b) and Fig. 14(c), respectively. Irreversible demagnetization of some points has occurred and magnetic flux density of PMs is decreased gradually during the discharge process and it is recovered after discharge. The most serious demagnetization points are circled as shown in Fig. 14. Flux density distribution of PMs at the end of discharge is shown in Fig. 14 (d), and the results show that the demagnetization of PMs with radial magnetization direction is more serious.

IV. Thermal Rise Demagnetization

The magnetic properties of PMs vary with temperature, but the effect of the same temperature rise on their properties is different at different temperatures. The magnetic properties of PM is related to coercivity, remanence, temperature coefficient, and intrinsic coercivity. In this section, the effect of different temperature on the demagnetization of Halbach array PM and the performance of CPA is studied by using finite element software when the CPA operates in different states, and temperature rise demagnetization of PMs is achieved by setting a temperature value to all PM blocks. The demagnetization of PMs can be analyzed more accurately by the bidirectional coupling analysis of electromagnetic field and temperature field.

A. Estimation of Temperature Rise Demagnetization

Temperature rise is one of the main factor affecting the demagnetization of PMs. In this section, the demagnetization risk of PM at different temperatures is estimated by analytic formula based on intrinsic demagnetization curve. The analytical calculation model as shown in Fig. 15.

Refer to [15], the functional relationship between remanence B_r, intrinsic coercivity H_{ci}, and reference temperature t_0 at any temperature can be approximately expressed as a polynomial relationship as follows

$$\begin{cases} B_r(t) = B_r(t_0)\left[1+\alpha_1(t-t_0)+\alpha_2(t-t_0)^2\right] = B_r(t_0)P(t) \\ H_{ci}(t) = H_{ci}(t_0)\left[1+\beta_1(t-t_0)+\beta_2(t-t_0)^2\right] = H_{ci}(t_0)Q(t) \end{cases} \quad (2)$$

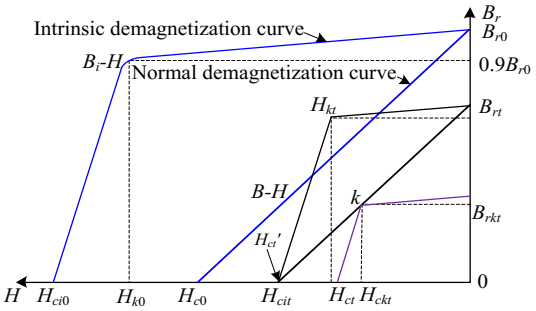

Fig. 15. Linear calculation model of temperature rise demagnetization based on intrinsic demagnetization curve.

The permeability $\mu(t)$ of the recoil line for demagnetization curve at any temperature is calculated by using (3).

$$\mu(t)=\left.\frac{\partial B_i(H,t)}{\partial H}\right|_{H=0}+\mu_0=\frac{P(t)}{Q(t)}\mu_i(t_0)+\mu_0 \tag{3}$$

where B_i is the intrinsic flux density, $B=B_i+\mu_0 H$, μ_0 is the permeability of the vacuum.

The variable k is the ratio of flux density at knee point to remanence at the corresponding temperature, and it is usually used to represent the knee point. It is assumed that parameter D (means rectangularity coefficient) and the relative permeability of the recoil line is constant, and the value of the variable k is calculated by using (5). However, this method can only be used to evaluate the approximate global demagnetization of PMs, and it is difficult to determine the local demagnetization risk.

Based on the B_i-H as shown in Fig. 15, the remanence B_{rt} and the knee point (B_{rkt}, H_{ckt}) at any temperature can be calculated by

$$\begin{cases} B_{rt}=\left[1-\alpha_B(t-t_0)\right]B_{r0} \\ H_{cit}=\left[1-\alpha_H(t-t_0)\right]H_{ci0} \\ B_{rkt}=kB_{rt} \\ H_{ckt}=(1-k)B_{rt}/\mu \end{cases} \tag{4}$$

where μ is the permeability of the PM, H_{ci0}, B_{r0} are the intrinsic coercivity and remanence at reference temperature, respectively, and α_H, α_B are the absolute value of temperature coefficient of the intrinsic coercivity and remanence.

According to (4), the value of knee point is calculated as follows

$$k=1-\frac{\mu D\left[1-\alpha_H(t-t_0)\right]H_{ci0}}{\left[1-\alpha_B(t-t_0)\right]B_{r0}} \tag{5}$$

where $D=H_{k0}/H_{ci0}$ is the rectangularity coefficient of intrinsic demagnetization curve.

B. Effect of Temperature on No-Load Performance

In order to study the effect of temperature rise on the performance of PMs, the thermal demagnetization model is built. The magnetic performance of PMs is analyzed when the armature windings are open-circuit in this section. Simulation results of CPA at different temperatures are shown in Fig. 16, and magnetic field distribution of PMs at different temperatures as shown in Fig. 17.

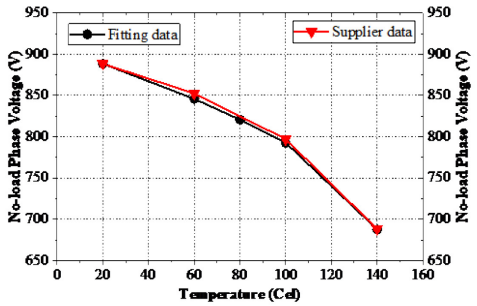

Fig. 16. Variations of no-load phase voltage before discharge with different temperatures.

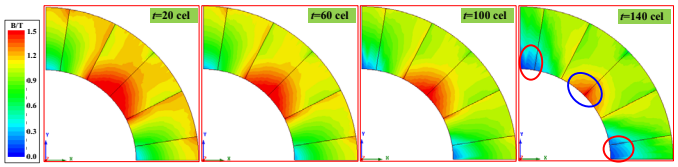

Fig. 17. No load flux density distribution of PMs at different temperatures.

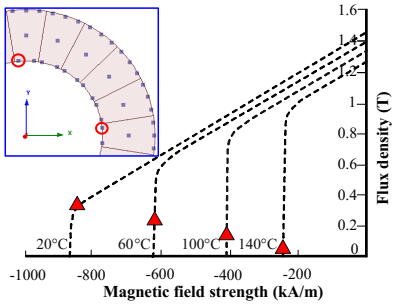

Fig. 18. The lowest working points of PMs at different temperatures during discharge.

According to curve of phase voltage versus temperature from Fig. 16, the phase voltage is decreased by temperature rise and the decreasing rate becomes slower gradually, and the phase voltage decreased by 14.9% at 140°C. The magnetic properties of PMs will decrease because of the great influence of temperature rise. The lowest operating points of PMs at different temperature are shown in Fig. 17. The operating point runs below the knee point at 100°C, and the irreversible demagnetization of PMs has occurred. The working temperature of PMs should not exceed 100°C.

C. Effect of Temperature Rise on Discharge Demagnetization

The thermal demagnetization of PMs with winding discharge involves the armature reaction and external magnetic field demagnetization, and the demagnetization effect is so complicated. Variations of no-load phase voltage after discharge, load current with different temperatures as shown in Fig. 19, and magnetic field distribution of PMs after discharge at different temperature as shown in Fig. 20.

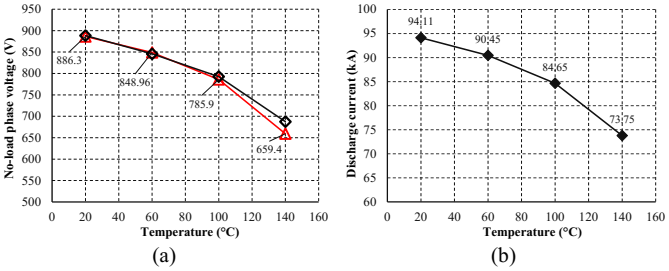

(a) (b)

Fig. 19. Variations of no-load voltage after discharge and load current with different temperatures. (a) No-load phase voltage. (b) Discharge current.

The higher temperature, the greater difference of no-load voltage value before and after discharge from variation of no-load phase voltage are shown in Fig. 19(a), and the difference is about 4.08% at 140°C. The results indicate that PM becomes easier to demagnetize due to the increase of temperature. The discharge ability of CPA decreases faster with the increase of the ambient temperature from Fig. 19(b). The research results show that the higher temperature, more serious demagnetization of PM. Load current waveforms of two-phase winding discharge with different temperatures as shown in Fig. 21.

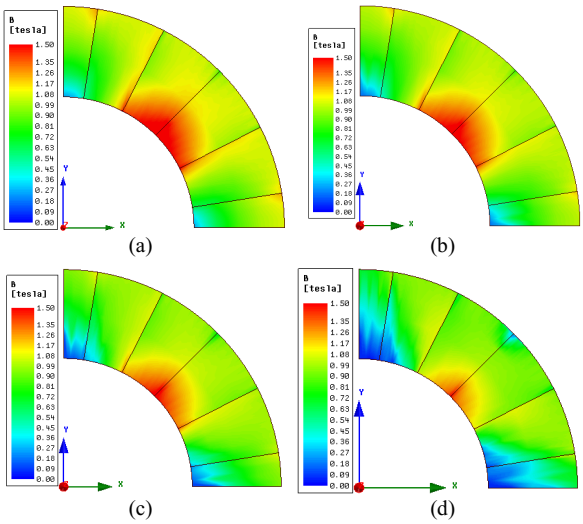

Fig. 20. No-load flux density distribution of PMs after discharge with different temperatures. (a) 20°C. (b) 60°C. (c) 100°C. (d) 140°C.

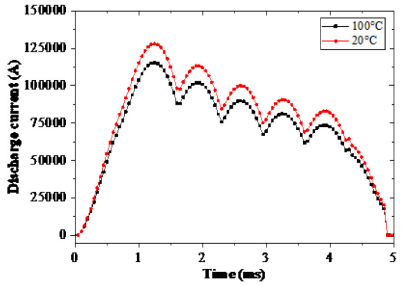

Fig. 21. Comparison of load current waveforms for two-phase winding discharge at 20°C and 100°C.

Based on the simulation result as shown in Fig. 21, the average value of load current for multiphase winding discharge at 100 °C is about 10.3% lower than that at 20°C. Comparison of load current for two-phase winding discharge indicates that multiphase winding discharge will further increase the demagnetization risk of PMs at high temperature.

V. Conclusions And Discussions

The demagnetization behaviors of PMs in the Halbach magnetized CPA is analyzed by linear demagnetization model. The research results indicate that the compensating shield can not only increase the discharge current, but also weaken the effect of armature reaction on the demagnetization of PM. Multiphase winding discharge increases the demagnetization risk of PMs. The fitting model of coercivity and remanence with different temperatures has a high accuracy. The ambient temperature of PM should not exceed 100 °C in order to ensure the operation of CPA. The research work can be used as the guidance for demagnetization analysis of PM pulsed alternator.

In this paper, linear demagnetization model is used into demagnetization research of Halbach magnetized pulsed alternator, but there is a certain difference from the actual demagnetization of Halbach array PMs. The demagnetization behaviors of PMs can be analyzed more accurately by the bidirectional coupling analysis of electromagnetic field and temperature field in future. Although the finite element software is perfect enough, how to verify the accuracy and correctness of simulation analysis through actual experiments is worthy of further study.

References

[1] I. R. McNab, “Electromagnetic space launch considerations,” *IEEE Trans. Plasma Sci.*, vol. 46, no. 10, pp. 3628-3633, Oct. 2018.

[2] I. R. McNab, “Pulsed power options for large EM launchers,” *IEEE Trans. Plasma Sci.*, vol. 43, no. 5, pp. 1352-1357, May 2015.

[3] I. R. McNab, “Large-scale pulsed power opportunities and challenges”, *IEEE Trans. Plasma Sci.*, vol.42, pp. 1118-1127, May 2014.

[4] M. Brennan, W. L. Bird, *et al.*, “The mechanica1 design of a compensated pulsed alternator prototype,” *in Proc. 2nd IEEE Int. Pulsed Power Conf.*, Texas Tech University, Lubbock, Texas, June 12-14. 1979.

[5] M. L. Spann, S. B. Pratap, *et al.*, “Rotating machines-power supplies for the next generation of EM accelerators,” *IEEE Trans. Magn.*, vol. 27, no. 1, pp. 344-349, Jan., 1991.

[6] M. L. Spann, S. B. Pratap, *et al.*, “Compulsator research at The University of Texas at Austin-an overview,” *IEEE Trans. Magn.*, vol. 25, no. 1, pp. 529-537, Jan. 1989.

[7] I. R. McNab, “Developments in pulsed power technology,” *IEEE Trans. Magn.*, vol. 37, no. 1, pp. 375-378, Jan. 2001.

[8] J. R. Kitzmiller, S. B. Pratap, and M. D. Driga, “An application guide for compulsators,” *IEEE Trans. Magn.*, vol. 39, no. 1, pp. 285-288, Jan. 2003.

[9] C. Ye, K. Yu, Z. Lou, and Y. Pan, “Investigation of self-excitation and discharge processes in an air-core pulsed alternator,” *IEEE Trans. Magn.*, vol. 46, no. 1, pp. 150-154, Jan. 2010.

[10] D. J. Wehrlen, R. A. Lee and R. F. Thelen, “Power electronics and controls for air core compulsator,” *IEEE Trans. Magn.*, vol. 31, no. 1, pp. 90-95, Jan. 1995.

[11] X. Liu, K. Liu, *et al.*, “Design and fabrication of a PM excitation compulsator,” in *Proc. ICEMS*, Nanjing, 2005, pp. 778-781, vol. 1.

[12] S. Wu, S. Wu, S. Cui, *et al.*, “Design and analysis of a high-speed permanent magnet compensated pulsed alternator,” *IEEE Trans. Plasma Sci.*, vol. 45, no. 7, pp. 1314-1320, July 2017.

[13] S. Wu, W. Zhao, S. Wu, *et al.*, “Design and analysis of counter-rotating dual rotors permanent magnet compensated pulsed alternator,” *IEEE Trans. Plasma Sci.*, vol. 45, no. 7, pp. 1101-1107, July 2017.

[14] A. Sarikhani and O. A. Mohammed, “Demagnetization control for reliable flux weakening control in pm synchronous machine,” *IEEE Trans. on Energy Convers.*, vol. 27, no. 4, pp. 1046-1055, Dec. 2012.

[15] P. Zhou, D. Lin, *et al.*, “Temperature-dependent demagnetization model of PMs for finite element analysis,” *IEEE Trans. Magn.*, vol. 48, no. 2, pp. 1031-1034, Feb. 2012.

[16] J. D. McFarland and T. M. Jahns, “Investigation of the rotor demagnetization characteristics of interior pm synchronous machines during fault conditions,” *IEEE Trans. Ind. Appl.*, vol. 50, no. 4, pp. 2768-2775, July-Aug. 2014.

[17] K. Kim, Y. Lee and J. Hur, “Transient analysis of irreversible demagnetization of permanent-magnet brushless dc motor with interturn fault under the operating state,” *IEEE Trans. Ind. Appl.*, vol. 50, no. 5, pp. 3357-3364, Sept.-Oct. 2014.

Songlin Wu was born in Zunyi, Guizhou, China, in 1992. He received the bachelor's degree and the M.Sc. degree in electrical engineering from the Harbin Institute of Technology (HIT), Harbin, China, in 2015 and 2017, where he is currently pursuing the doctor's degree.

He specializes in the research field of hybrid excitation compulsators, including the machine design and multiphysics field analysis. His current research interests include drive and control of micro special electric machines.

Shaopeng Wu (S'10–M'11-SM'19) was born in Linkou, Heilongjiang, China, in 1983. He received the B.S., M.S., and Ph.D. degrees in electrical engineering from the Harbin Institute of Technology (HIT), Harbin, China, in 2005, 2008, and 2011, respectively.

He was a Visiting Scholar of Wisconsin Electric Machines and Power Electronics Consortium (WEMPEC) with the University of Wisconsin-Madison, Madison WI, USA, from 2013 to 2014. He is currently an Associate Professor with HIT. His current research interests include the design and control of special electric machines, the research of multiphysical coupling, and the related technologies in electromagnetic launch field.

Dr. Wu has been a member of the IEEE Magnetics Society and the IEEE Nuclear and Plasma Sciences Society since 2011. He was a recipient of the Peter J. Kemmey Memorial Scholarship by the 15th International EML Symposium, Brussels, Belgium, in 2010.

Weiduo Zhao was born in Harbin, China, in 1985. He received the bachelor's degree in electrical engineering from the Taiyuan University of Technology, Taiyuan, China, in 2008, and the M.Sc. degree and Ph.D degree in electrical engineering from the Harbin Institute of Technology, Harbin, China, in 2010 and 2015, respectively.

He is currently a senior research fellow with the Power Electronics, Machines and Control Group, The University of Nottingham, Ningbo, China. His research interests include high-performance electric machines and drives, pulsed power systems, and thermal management.

Dr. Zhao was a recipient of the Peter J. Kemmey Memorial Scholarship from the 17th International Electromagnetic Launch Symposium, San Diego, CA, USA, in 2014.

Shumei Cui was born in Yichun, Heilongjiang, China, in 1964. She received the Ph.D. degree in electrical engineering from the Harbin Institute of Technology (HIT), Harbin, China, in 1998.

She has been a Professor with the Department of Electrical Engineering, HIT, where she is currently the Vice Dean of the Institute of Electromagnetic and Electronic Technology and the Dean of the Electric Vehicle Research Centre. Her current research interests include design and control of micro and special electric machines, electric drive system of electric vehicles, control and simulation of hybrid electric vehicles, and intelligent test and fault diagnostics of electric machines.

Prof. Cui serves as the Vice Director Member of the Micro and Special Electric Machine Committee and the Chinese Institute of Electronics, and a member of the Electric Vehicle Committee and the National Automotive Standardization Technical Committee.